Green Chemistry

PAPER

View Article Online
View Journal | View Issue

Cite this: *Green Chem.*, 2025, **27**, 2102

Synthesis of CO_2-based biomass derived non-isocyanate polyurethane hybrid adhesives with excellent mechanical properties and water resistance†

Ping Zhang, Chen Qin, Hao Yuan, Yu Wang, Yizhong Cao, Zhe Wang * and Chunde Jin*

The increasing focus on reducing greenhouse gas emissions and the utilization of biomass resources have driven significant interest in developing environmentally friendly, non-toxic, non-isocyanate polyurethane (NIPU) adhesives derived from CO_2 and green resources. However, the mechanical properties of NIPUs are much inferior to those of traditional isocyanate-based polyurethanes, thereby restricting their applicability in adhesives and other fields. Therefore, it is imperative to find a solution for the pressing problem of how to enhance their mechanical properties utilizing biomass resources for broadening their large-scale applications. In this work, linear NIPU prepolymers with amine-terminal groups were promptly synthesized at ambient temperature, utilizing biomass cashew phenol diglycidyl ether (602A) and bio-oil-based diamines (Priamine 1074) as raw materials. To enhance the mechanical properties of NIPU prepolymers, ethanol fractionation was utilized to extract small-molecule lignin (EFL) from enzymatic hydrolysis lignin (EHL). Subsequently, EFL was synthesized into lignin-based epoxy resin (LEP) *via* a solvent-free process, and then grafted onto the amine-terminated NIPUs to form a three-dimensional network structure of lignin-based epoxy resin hybrid non-isocyanate polyurethanes (LEP-NIPUs). LEP-NIPU polymers with the epoxy resin as the rigid segment and NIPUs as the flexible segment not only possess superior mechanical properties including tensile strength of up to 20.01 MPa but also have excellent hydrophobicity and corrosion resistance to seawater. These properties contributed to a wet shear strength of 2.31 MPa when applied as wood adhesives, indicating promising application prospects for the future development of underwater adhesives.

Received 23rd October 2024,
Accepted 14th January 2025

DOI: 10.1039/d4gc05323k

rsc.li/greenchem

Green foundation

1. Polyurethanes are an indispensable material in industrial production. We have proposed to utilize biomass materials and CO_2 to synthesize green non-isocyanate polyurethane adhesives that are non-toxic and free of formaldehyde release.
2. When the adhesives are applied to plywood, it has excellent bonding strength and excellent water resistance. It is expected to replace traditional formaldehyde-based adhesives and reduce the emission of formaldehyde gas.
3. During the synthesis of cyclic carbonates from CO_2, high temperatures are currently indispensable. The key question that lies ahead for us in our endeavor to curtail energy emissions is how to facilitate the reaction between CO_2 and epoxides under relatively low temperatures.

1. Introduction

Due to the swift expansion of the artificial board industry, the consumption of wood adhesives has become an essential indicator of its development level.[1] Urea-formaldehyde resins, phenol-formaldehyde resins, and other formaldehyde-based adhesives maintain a dominant position in the adhesives market due to their excellent bonding performance, accounting for more than 90% of the adhesives used in artificial boards.[2–4] However, formaldehyde-based adhesives not only deplete considerable amounts of fossil raw resources during production, but also release free formaldehyde, which causes environmental contamination and poses serious health risks.[5,6] In recent years, polyurethane (PU) adhesives have attracted considerable attention in the coatings and adhesives sectors because of their notable

Bamboo Industry Institute, Zhejiang A & F University, Hangzhou 311300, PR China. E-mail: wangzhe@zafu.edu.cn, jincd@zafu.edu.cn

† Electronic supplementary information (ESI) available. See DOI: https://doi.org/10.1039/d4gc05323k

advantages, including formaldehyde-free emission, exceptional adhesion strength, and weather resistance.[7–9] Nonetheless, the advancement of PU adhesives faces considerable restrictions, primarily due to the requirement of incorporation of highly toxic isocyanates during their manufacturing process.[10]

Confronted with the soaring CO_2 concentration, challenges such as global warming, extreme weather, and ecosystem collapse are becoming increasingly severe.[11,12] As a C1 resource with the characteristics of non-flammability, non-toxicity, and renewability, CO_2 offers innovative opportunities for energy conservation, emission reduction, and the evolution of cutting-edge energy technologies.[13] One of the most effective strategies in this regard is the synthesis of five-membered cyclic carbonates from CO_2 and epoxy compounds.[14] Additionally, the harnessing of CO_2 for the synthesis of cyclic carbonates undoubtedly opens new possibilities for advancing sustainable development in NIPUs manufacturing.[15] NIPUs are a category of polymeric materials synthesized through the interaction of five-membered cyclic carbonates with amines, resulting in a chain of carbamate units.[16]

In contrast to traditional PUs, NIPUs facilitate the high-value utilization of biomass feedstocks and CO_2 while eliminating safety risks associated with isocyanates during manufacturing and application processes.[17,18] The most commonly used biomass materials currently include vegetable oils, terpenoids, rosin compounds, and agricultural waste.[19–22] As a natural phenolic compound, cashew phenol and its derivatives possess special chemical structures that endow it with high-temperature resistance, enhanced toughness, and other remarkable properties. These characteristics create favorable conditions for the synthesis of multifunctional, high-performance NIPU adhesives.[23,24] Currently, cashew phenol and its derivatives have gained broad applications in the synthesis of epoxy resins, benzoxazines, and other compounds.[25,26] However, there are few reports on the synthesis of CO_2-based cyclic carbonates using cashew phenol and its derivatives. A commercialized cashew phenol diglycidyl ether (602A), which contains two epoxy groups, can react with CO_2 to synthesize cashew phenol cyclic carbonates (CPCC) with two five-membered cyclic carbonate groups. The CPCC can then be synthesized into linear NIPUs by reacting with amines.

However, the mechanical properties of NIPUs are significantly inferior to those of traditional PUs, primarily due to bond exchange reactions between hydroxyl groups and carbamate bonds during the NIPU synthesis process, which is the primary challenge that needs to be addressed for NIPUs to replace traditional PUs in future development.[27] Currently, several strategies have been proposed to improve the mechanical properties of NIPUs. For instance, some researchers have suggested introducing hyperbranching structures to increase the cross-linking density within NIPUs, thus enhancing their mechanical strength. Others recommend incorporating rigid amines to improve the mechanical properties of NIPUs.[28,29] Furthermore, several studies have demonstrated that grafting rigid epoxy resins into NIPUs contributes to significant improvements in their mechanical properties.

This approach is particularly attractive for material design in the final 3D hybrid network with a defined sequence of soft segments (NIPUs) and hard segments (epoxy).[30] For instance, Ke Jiexi *et al.* synthesized polyurethanes/epoxy hybrid materials by curing NH_2-terminated non-isocyanate polyurethane pre-polymers with diglycidyl ether of bisphenol-A (BADGE);[31] He Xin *et al.* investigated the impact of different epoxy resins (E51 or E44) on the crosslinking density of NIPU prepolymers and discovered that synthetic HNIPU coatings modified with epoxy resins exhibited excellent impact resistance, pencil hardness, and other properties.[32]

Although the incorporation of epoxy resins enhances various properties of NIPUs, there are still many drawbacks, including the fact that the majority of the synthetic raw materials for the introduced epoxy resins are still derived from petroleum. Lignin, a naturally abundant and cost-effective polymer with a three-dimensional network structure, is composed of three types of phenylpropane units connected through ether bonds and carbon–carbon bonds.[33] Its molecular structure primarily contains functional groups such as methoxy groups, aliphatic and phenolic hydroxyl groups and so on. The presence of these functional groups in lignin enables various chemical reactions, thereby providing multiple avenues for its high-value utilization. As a result of the existence of the aromatic ring structure and phenolic groups, it exhibits rigidity, hydrophobicity, flame retardancy, and UV resistance, among other properties.[34–36] Consequently, the modification of NIPUs with lignin-based epoxy resins not only significantly improves the mechanical strength but also imparts additional advantageous properties, such as enhanced water resistance, *etc*.

This study aims to design and synthesize green NIPU adhesives with strong bonding strength and excellent water resistance. A commercialized cashew phenol derivative (602A) and CO_2 were initially selected to synthesize cashew phenol cyclic carbonate (CPCC), which was then cured with bio-oil-based diamines (Priamine 1074) to synthesize biomass-based linear NIPUs. For enhancing the mechanical strength of NIPUs, lignin was used to synthesize the lignin-based epoxy resin and subsequently grafted onto the NIPUs, constructing an adhesive with a cross-linked network structure that featured the epoxy resin as the rigid segments and the NIPUs as the flexible segments. The cross-linked network not only provides superior mechanical properties to the adhesive but also imparts excellent waterproofing and exceptional seawater corrosion resistance capabilities, thereby improving the wet bonding strength of wood adhesives and achieving exceptional adhesion in marine environments. On the one hand, this research can promote the green transformation of the industrial and energy structures of polyurethane adhesives; on the other hand, it also provides reference and technical support for the development of a green adhesive industry chain.

2. Experimental section

2.1. Lignin fractionation

Lignin fractionation was carried out by continuously stirring 100 g of EHL in a beaker containing 1000 mL of ethanol at

room temperature for 1 h. Subsequently, the dissolved and undissolved fractions were separated by centrifugation. The dissolved lignin (EFL) was further collected by rotary evaporation. The yield of lignin separated from ethanol can reach up to 50%, and the ethanol utilization rate by rotary evaporation can reach approximately 90%, allowing for recycling in subsequent lignin fractionation.

2.2. Synthesis of lignin epoxy resin

In brief, 10 g of EFL was added to a three-necked flask containing 60 g of epichlorohydrin, 0.1 g of TMAC, and 0.1 g of H_2O. As depicted in Fig. 1a and Fig. S1 of the ESI,† the excellent solubility of EFL in epichlorohydrin after ethanol fractionation eliminates the need for additional solvents in the whole reaction system. After the reaction system was continuously stirred at 100 °C for 4 h to initiate the phase-transfer reaction, 4.3 g of 20 wt% NaOH aqueous solution was added dropwise to the mixture under vigorous stirring, and the reaction continued for another hour at 100 °C to complete the ring-closing reaction. Once the reaction was complete, the mixture was cooled to room temperature, and deionized water was introduced to precipitate the epoxy compounds. The precipitated product was then vacuum filtered and washed several times with deionized water to remove residual reaction impurities, including

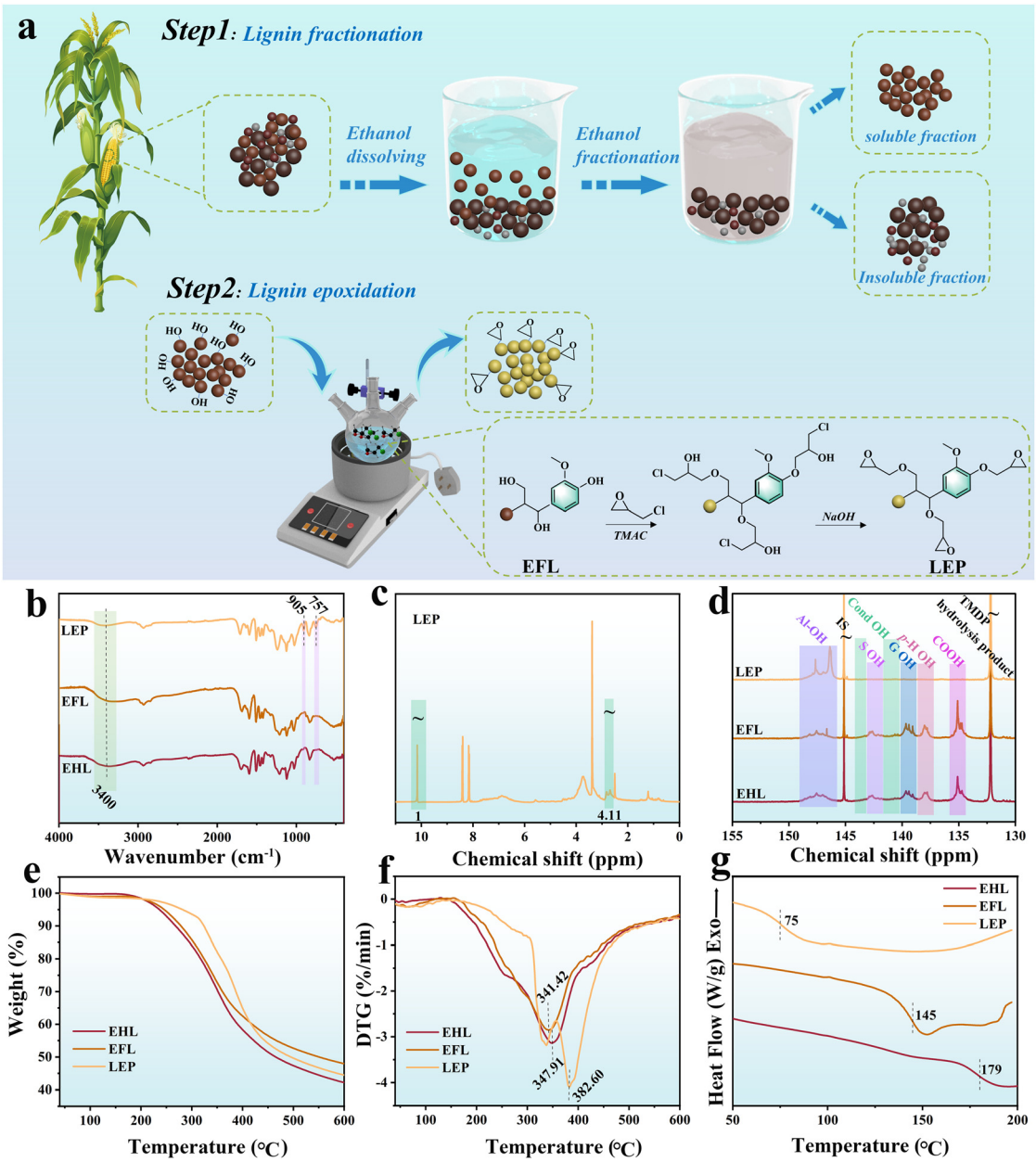

Fig. 1 (a) Schematic diagram of lignin fractionation and lignin epoxidation; (b) FTIR spectra of EHL, EFL, and LEP; (c) ^{1}H NMR spectrum of LEP; (d) ^{31}P NMR spectra, (e) TG curves, (f) DTG curves, and (g) DSC curves of EHL, EFL, and LEP.

sodium hydroxide, sodium chloride, TMAC, and any unreacted epichlorohydrin. Subsequently, the purified product underwent freeze-drying to yield the yellow lignin-based epoxy resin (LEP). The photographs of samples including EHL, EFL and LEP are shown in Fig. S2 of ESI.†

2.3. Synthesis of amine-terminated NIPU prepolymers

Briefly, the synthesis procedure was as follows. Firstly, 24 g of 602A and 1 wt% TEBA were added to a 50 mL high-pressure reactor (Beijing Huotong Experimental Instrument Co., Ltd). CO_2 was introduced and then vented three times to remove air from the apparatus. Subsequently, CO_2 was reintroduced until the internal pressure stabilized at 2 MPa. The reaction was carried out at 110 °C with mechanical stirring at 500 rpm. After the reaction was completed and cooled to room temperature, the product was transferred to a vacuum oven to eliminate excess CO_2. The cyclic carbonate equivalent weight was determined to be 0.3653 mol per 100 g. Amine-terminated NIPU prepolymers were synthesized according to the proportions outlined in Table 1. Priamine 1074 (1.35 g) was reacted with varying amounts of CPCC (0.96, 0.82, 0.68, and 0.55 g) at room temperature for 10 min to produce a series of amine-terminated NIPU prepolymers, which were designated as NIPU-1, NIPU-2, NIPU-3, and NIPU-4, respectively. The photographs of samples including Priamine 1074, 602A, CPCC, and NIPU prepolymers are shown in Fig. S3 of the ESI.†

2.4. Synthesis of LEP-NIPU adhesives and films

2.4.1. Synthesis of LEP-NIPU adhesives. According to the proportions in Table 1, a defined quantity of LEP was added to the synthetic NIPU prepolymers and thoroughly stirred at room temperature to ensure the complete reaction between the terminal amine groups of the NIPU prepolymers and the epoxy groups of the LEP. The resulting synthesized products were designated as LEP-NIPU$_{30:70}$, LEP-NIPU$_{40:60}$, LEP-NIPU$_{50:50}$ and LEP-NIPU$_{60:40}$, respectively.

2.4.2. Synthesis of LEP-NIPU films. To avert the formation of bubbles during the curing process, a small amount of solvent was added to the preparation process of the LEP-NIPU films for dissolution. According to the proportions in Table 1, the specific amount of LEP was dissolved directly in 5 mL of DMAC. Subsequently, it was added to the synthesized NIPU prepolymers and stirred homogeneously to guarantee a complete reaction between the terminal amine groups of NIPU prepolymers and the epoxy groups of LEP. The prepolymers were then poured into a polytetrafluoroethylene mold and cured at 140 °C for 6 h. Based on the molar ratio between the cyclic carbonate groups and the epoxy groups, the synthesized products were designated LEP-NIPU$_{30:70}$ film, LEP-NIPU$_{40:60}$ film, LEP-NIPU$_{50:50}$ film, and LEP-NIPU$_{60:40}$ film.

2.5. Bonding performance test

The specimen preparation and shear strength testing were conducted following the method described by Li *et al.*[37] Poplar veneers with dimensions of 200 mm × 62.5 mm × 2 mm (radial × tangential × longitudinal) were utilized as the sample materials for adhesive strength testing. The lap area was set at 200 mm × 25 mm, with the glue applied at 190 g m^{-2}. Subsequently, the boards were left at room temperature for 10 min and then hot-pressed for 15 min at 140 °C and 1.5 MPa. After being placed at ambient temperature and pressure for 24 h to release stress, the prepared plywood was cut into specimens with dimensions of 100 mm × 25 mm (testing area = 25 mm × 25 mm). For the wet shear strength test, the specimens were first immersed in water at 63 °C for 3 h, and then cooled for 10 min before testing. The bonding performance test was repeated six times for each sample using the universal testing machine (Instron5960, USA) equipped with a 10 kN load cell at a tensile speed of 5 mm min^{-1}.

3. Results and discussion

The characteristic functional groups of EHL, EFL, and LEP were analyzed by FTIR spectroscopy, as exhibited in Fig. 1b. It can be observed that the functional groups of EHL exhibit no significant alterations, which implies that the structure remains relatively stable during the ethanol fractionation process. A board absorption band spanning from 3500 to 3250 cm^{-1} is associated with the O–H stretching vibrations of both phenolic and aliphatic hydroxyl groups.[38] The stretching vibration peaks at 2932 cm^{-1} and 2833 cm^{-1} are correspondingly related to –CH_3 and –CH_2– groups, respectively. The absorption peaks at 1704 cm^{-1} signify the C=O stretching vibrations in lignin. The absorption peaks at 1603 cm^{-1}, 1513 cm^{-1}, and 1425 cm^{-1} are attributed to the vibrations of the aromatic ring skeleton of lignin.[39] The absorption peak at 1267 cm^{-1} corresponds to the C=O regular stretching vibration of the G unit within lignin.[40] The absorption peak at 979 cm^{-1} is assigned to the C–H bending vibrations outside the aromatic ring of the G unit.[41] Additionally, the absorption peak at 1128 cm^{-1} is assigned to the C–H deformation vibration within the ring of the S-unit, while the absorption

Table 1 The synthetic ratios of samples

Sample	CPCC (mol)	Priamine 1074 (mol)	LEP (mol)	CPCC (g)	Priamine 1074 (g)	LEP (g)
LEP-NIPU$_{30:70}$	0.0035	0.005	0.0015	0.96	1.35	0.57
LEP-NIPU$_{40:60}$	0.003	0.005	0.002	0.82	1.35	0.75
LEP-NIPU$_{50:50}$	0.0025	0.005	0.0025	0.68	1.35	0.94
LEP-NIPU$_{60:40}$	0.002	0.005	0.003	0.55	1.35	1.13

peak at 838 cm^{-1} is attributed to the C–H bending vibration outside the C_2 and C_6 faces of the S-unit.[42,43]

Due to the varying solubility of lignin in ethanol, the soluble lignin fractions typically exhibit lower molecular weights compared to the insoluble fractions.[44] This observation has been further supported by testing and analysis of the molecular weight distribution of lignin. As depicted in Fig. S4–6 of the ESI† and Table 2, EHL possesses a weight-average molecular weight (M_w) of 4780 g mol^{-1}, which is one order of magnitude higher than that of EFL (2110 g mol^{-1}). Additionally, EFL exhibits a more concentrated molecular weight distribution than EHL. As shown in Fig. S4 and S5 of the ESI,† the relatively lower molecular weight and narrower distribution of EFL contribute to its enhanced solubility in epichlorohydrin, facilitating the epoxidation reaction without the need for additional solvent. Consequently, lignin fractionation using ethanol is advantageous for the synthesis of lignin-based epoxy resins. After the epoxidation of lignin, a noticeable weakening in the broad hydroxyl peak is observed. The appearance of a characteristic peak corresponding to the epoxy group at 905 cm^{-1} indicates the successful epoxidation of lignin.[45] In addition, the epoxy value of LEP was determined to be 2.65 mmol g^{-1} (Fig. 1c), which is comparable to those of lignin-based epoxy resins prepared from lignin derived *via* hydrogenolysis or steam explosion.[46,47] However, the ethanol fractionation method is safer and more cost-effective.

Quantitative ^{31}P NMR spectroscopy was employed to observe the variations in the surface hydroxyl groups composition during the processes of ethanol fractionation and epoxidation. As illustrated in Fig. 1d, the ^{31}P NMR spectrum can be categorized into three principal regions including the ranges of 150–145.4 ppm for aliphatic hydroxyl (aliphatic-OH) signal peak, 144–137.6 ppm for phenolic hydroxyl (Ph-OH) signal peak, and 136–133.6 ppm for carboxylic acid groups (COOH) signal peak, respectively.[48] More specifically, Ph-OH can be further divided into condensed (Cond), syringyl (S), guaiacyl (G), and *p*-hydroxyphenyl (*p*-H) OH.[49] In addition, the quantities of OH groups determined from the integral areas within each spectral region are provided in Table 2. Notably, the content of hydroxyl groups in lignin exhibits a significant correlation with its molecular weight. The total aliphatic OH content increases as the molecular weight increases, which is consistent with previous reports that lignin with lower molecular weight has fewer aliphatic hydroxyl groups compared to lignin with higher molecular weight.[50] Given that ethanol can provide stronger hydrogen bonding and polar interactions, the total amount of Ph-OH groups increases after ethanol fractionation. The quantities of S, G, and *p*-hydroxyphenyl OH exhibit an upward trend as the molecular weight decreases, whereas the amounts of Cond OH exhibit the opposite trend. Moreover, the COOH content in EHL and EFL can reach 1.11 mmol g^{-1} and 1.60 mmol g^{-1}, respectively, which is significantly higher than that reported for raw lignin, indicating that EFL exhibits excellent solubility. Furthermore, the content of COOH increases after ethanol fractionation, which aligns with the observation that EFL is completely dissolved in ethanol. Following the epoxidation process, the contents of Ph-OH and COOH decrease significantly, indicating the successful conversion of these functional groups into epoxides.

The thermal stability of EHL, EFL, and LEP was assessed using TGA under a nitrogen atmosphere. Fig. 1e and f clearly show that EHL and EFL underwent a continuous, and single-step degradation process, whereas LEP displayed a two-step thermal degradation pattern. The mass loss between 150 °C and 300 °C is attributed to the cleavage of α- and β-aryl–alkyl ether bonds.[51] The aliphatic side chains of lignin are detached and severed from the aromatic rings, resulting in the exposure of a greater number of aldehyde and phenolic groups at about 300 °C.[42] The breakdown of C–C interunit bonds between lignin structural units occurred within the temperature range of 350–450 °C.[52] Ultimately, the aromatic rings of lignin underwent decomposition or condensation reactions as the temperature increased from 400 °C to 600 °C.[53] The $T_{5\%}$ (5% weight loss) for EHL and EFL occurred at 235.82 °C and 226.87 °C, respectively, indicating rapid thermal degradation as molecular weight decreases.[48,54] The T_s values of EHL and EFL are 149.66 °C and 148.21 °C, respectively, showing little difference between them. However, LEP exhibits higher values for $T_{5\%}$ (281.32 °C), $T_{30\%}$ (387.32 °C), T_s (169.01 °C), and T_{max} (382.60 °C) compared to EHL and EFL. This implies that lignin achieves improved thermal stability following epoxidation (Table 3). Additionally, the glass transition temperature (T_g) of the lignin samples is also positively correlated with the molecular weight. The T_g value of EHL is 179 °C, while that of EFL is 145 °C. These results are attributed to the higher molecular weight of lignin, which contains more phenyl ring structures and rigid connections.[55] Upon epoxidation, the T_g value of LEP significantly decreases to 75 °C (Fig. 1g).

Table 2 The M_n, M_w, $Đ$, and hydroxyl group contents of the EHL, EFL, and LEP as determined using GPC and ^{31}P NMR analyses

		EHL	EFL	LEP
GPC results	M_n (g mol^{-1})	870	720	790
	M_w (g mol^{-1})	4780	2110	1600
	$Đ$ (M_w/M_n)	5.49	2.93	2.03
^{31}P NMR results	Cond OH	0.74	0.61	0.04
	S OH	0.43	0.57	0.02
	G OH	0.79	1.16	0.01
	p-H OH	0.63	0.91	0.01
	Total Ph-OH	2.59	3.25	0.08
	Aliphatic-OH	1.17	1.06	2.21
	COOH	1.11	1.60	0.01

Table 3 The TGA data for EHL, EFL, and LEP

Sample	$T_{5\%}$ (°C)	$T_{30\%}$ (°C)	T_s (°C)	T_{max} (°C)	C_{600} (%)
EHL	235.82	351.82	149.66	347.91	42.19
EFL	226.87	352.87	148.21	341.42	45.97
LEP	281.32	387.32	169.01	382.60	44.44

T_s was calculated using the equation: $T_s = 0.49\,[T_{5\%} + 0.6(T_{30\%} - T_{5\%})]$.

The molecular structures and interunit linkages of EHL, EFL, and LEP were characterized using 2D-HSQC spectroscopy, thereby analyzing the detailed structural alterations of lignin during the fractionation and epoxidation processes. Fig. 2 predominantly depicts the side chain and aromatic regions, with the principal signal assignments provided in Table S2 of the

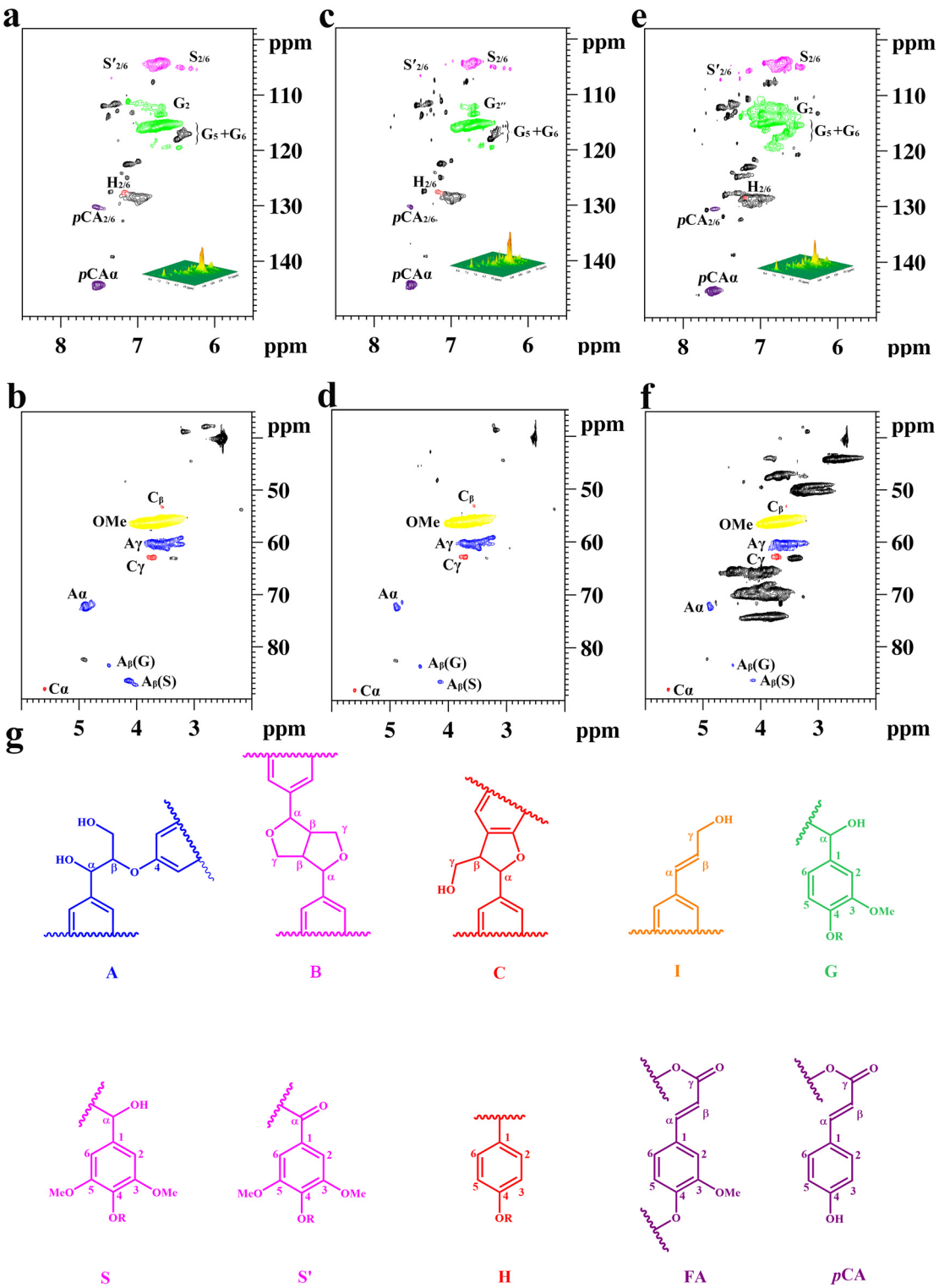

Fig. 2 2D HSQC NMR spectra of each lignin fraction. Side chain regions of (a) EHL, (c) EFL, (e) LEP and the aromatic regions of (b) EHL, (d) EFL, (f) LEP; (g) A: β-O-4 alkyl-aryl ethers, B: resinol, C: phenylcoumaran, I: *p*-hydroxycinnamyl alcohol end-group, G: guaiacyl unit, S: syringyl unit, S′: oxidized syringyl unit.

ESI.† The primary connected structures are shown in Fig. 2g. The characteristic groups and structural units of the lignin samples were integrated using a semi-quantitative method, and the relationship between molecular weight and structure of each lignin was studied. Since the lignin is derived from corn stalks, the content of the H unit is relatively low.[56] The abundance of the H unit remains nearly constant before and after ethanol fractionation. Nevertheless, the S unit presents a slight downward trend, while the G unit exhibits an upward trend. By analyzing the abundance of various linkages, it is observed that the β-O-4 linkages in lignin have decreased, while the β-5 linkages have shown a slight increase after ethanol fractionation. According to previous research, the ratio of flexible linkages (β-O-4) to rigid linkages (β-5) in lignin affects the toughness and strength of the lignin-based materials.[57] The analysis of linkage units reveals that the proportion of flexible linkage units has diminished following ethanol fractionation.

Fig. 3a presents the procedures for the synthesis of LEP-NIPUs. Firstly, cashew phenol diglycidyl ether (602A), which is derived from natural biomass materials, reacted with CO_2 at 110 °C and 2 MPa for 20 h to produce cashew phenol cyclic carbonate (CPCC). Subsequently, CPCC and the diamine (Priamine 1074) originating from biomass oil-based materials underwent a reaction at room temperature for 10 min according to the reaction ratios in Table 1 and the reaction principle in Fig. 3b, aiming to obtain NIPU prepolymers with terminal amine groups. In addition, in order to demonstrate that the synthesized NIPUs possess green properties, we conducted Life Cycle Assessment (LCA) analysis on them and petroleum-based NIPUs (the specific analysis is described in the ESI†). These NIPU prepolymers were then synthesized with LEP in varying stoichiometric ratios *via* the ring-opening reaction of primary amines with epoxy groups, resulting in a series of lignin-based epoxy resin hybrid polyurethanes (LEP-NIPUs) with adjustable properties, as shown in Fig. 3c.

Fig. 4a displays the ^{1}H NMR spectra of 602A, CPCC synthesized at 7 h and 20 h. Noticeably, there is a progressive attenuation of the peak intensity within the range of 2.90–3.40 ppm, which corresponds to the epoxy group. Meanwhile, the peaks for cyclic carbonates appear at 4.6 ppm. These changes indicate that 602A has successfully reacted with CO_2.[58] Meanwhile, the peak has completely disappeared after 20 h compared to the reaction at 7 h, which proves that all epoxy groups have been fully converted into cyclic carbonate groups. In addition, the FTIR spectra of 602A, CPCC, and Priamine 1074 are shown in Fig. 4b. For 602A, the absorption peak at 910 cm^{-1} is attributed to the epoxy group and the C–H out-of-plane bending absorption peaks of the terminal vinyl group.[59] The absorption peak at 1795 cm^{-1} corresponds to the C═O stretching vibration resulting from the ring-opening of epoxy groups. These results demonstrate the successful conversion of epoxy groups into cyclic carbonate groups.[60] The FTIR

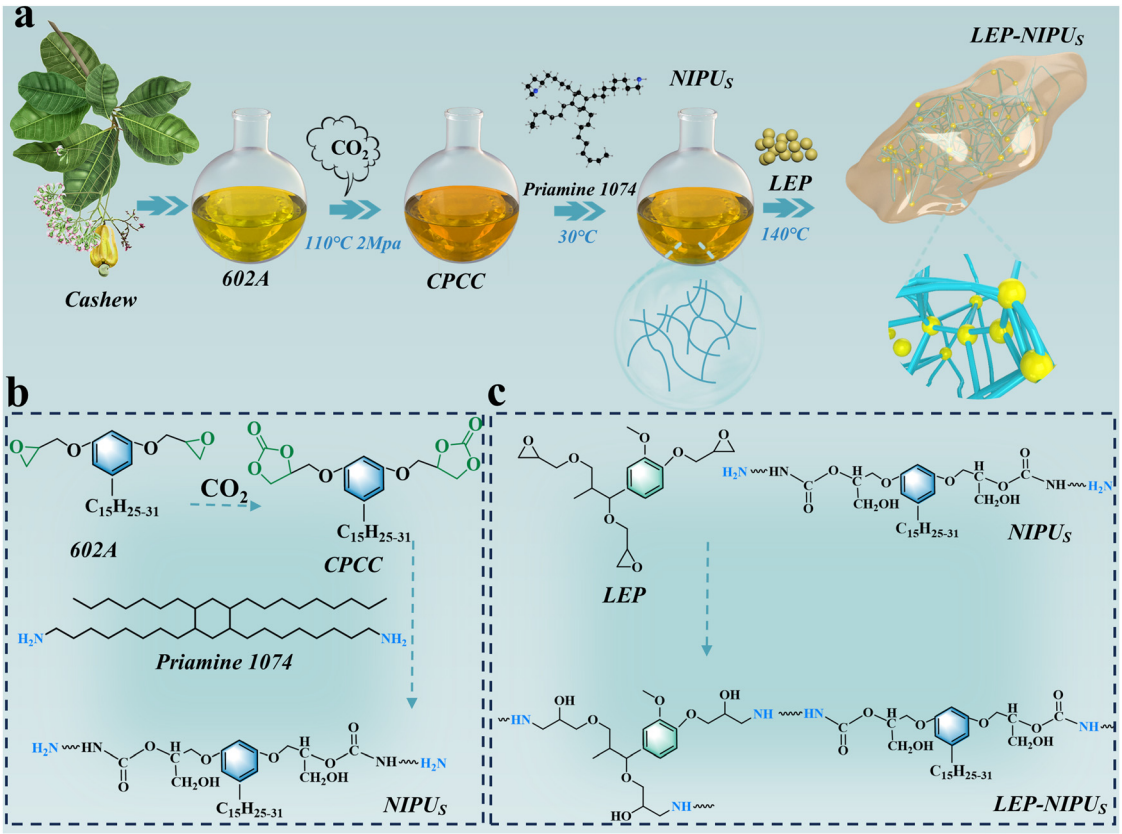

Fig. 3 (a) Reaction steps of LEP-NIPUs; (b and c) synthetic routes of NIPUs and LEP-NIPUs.

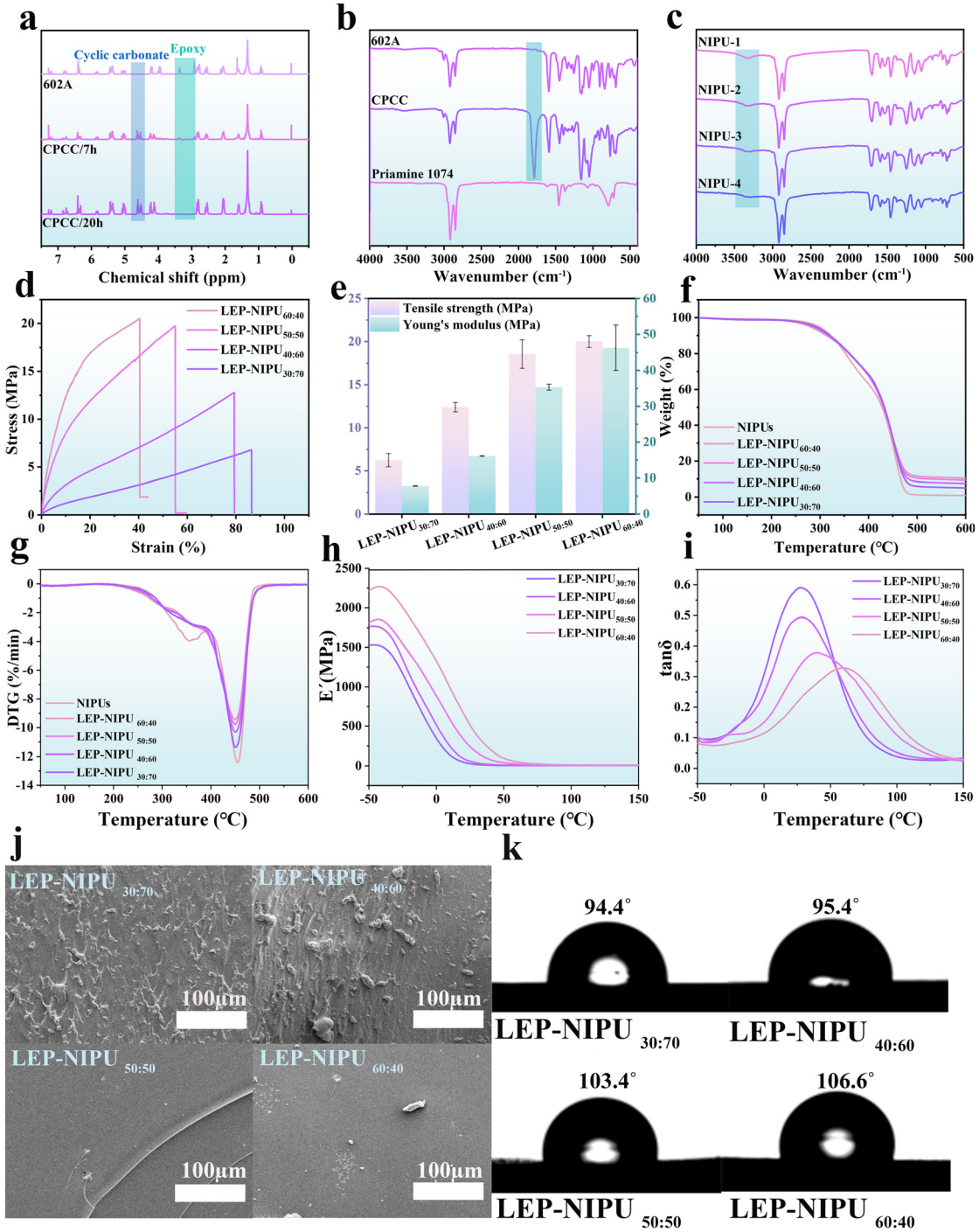

Fig. 4 (a) ^{1}H NMR spectra of 602A and CPCC synthesized at 7 h and 20 h; (b) FTIR spectra of 602A, CPCC, and Priamine 1074; (c) FTIR spectra of NIPU prepolymers; (d) tensile stress–strain curves of LEP-NIPUs films; (e) tensile strength and Young's modulus of LEP-NIPU films; (f) TG curves and (g) DTG curves of LEP-NIPU samples; (h) storage modulus curves and (i) tan δ curves of LEP-NIPU films; (j) SEM micrographs of fractured surfaces of LEP-NIPU films; (k) contact angle images of LEP-NIPU films.

spectra of the four LEP-NIPU prepolymers are shown in Fig. 4c. Following the ring-opening reaction of CPCC, the C=O bond at the peak of 1795 cm^{-1} vanishes. Simultaneously, the newly emerged characteristic peaks of NIPUs at 1710 and 1545 cm^{-1} are attributed to the C=O stretching vibration and N–H stretching vibration in the carbamate group, respectively.[61] Furthermore, the bending vibration of –OH from NIPUs appears at 3363 cm^{-1}. As the reaction ratio of cyclic carbonate to amine groups continuously increases, the intensity of the hydroxyl peak correspondingly also increases.[62] These results confirmed that CPCC and Priamine 1074 successfully synthesized the NIPU prepolymers.

Different LEP-NIPUs films exhibit a range of distinct physical properties. For instance, the LEP-NIPU$_{50:50}$ rectangular film (0.83 g, 50 mm × 10 mm × 0.5 mm) could easily lift a 1.5 kg heavy object, thereby demonstrating its excellent mechanical properties (see Fig. S7, ESI†). The mechanical properties of LEP-NIPUs films were evaluated by a uniaxial tensile test, and the corresponding tensile strength curves are presented in Fig. 4d. The results indicate that the tensile strength and Young's modulus of LEP-NIPU films increase with higher lignin epoxy resin content. The tensile strength and Young's modulus of LEP-NIPU$_{30:70}$ film can reach 6.23 MPa and 7.83 MPa, respectively, while those of LEP-NIPU$_{60:40}$ can reach 20.01 MPa and 46.31 MPa, respectively. The excellent mechanical performance of LEP-NIPUs is attributed to the formation of a robust cross-linked network derived from the amine-NIPU prepolymers and LEP. The SEM images of LEP-NIPU$_{30:70}$ film and LEP-NIPU$_{40:60}$ film reveal rough fracture surfaces, suggesting an ability to absorb significant energy under external forces, indicative of high toughness. With the increment in the content of LEP, the fracture surfaces of LEP-NIPUs films gradually transition towards brittleness (Fig. 4j). The fracture surface of LEP-NIPU$_{50:50}$ is smooth with minimal cracks, which is a characteristic feature of brittle fractures. Additionally, when the molar ratio of LEP is increased to 60%, the fracture surface of LEP-NIPU$_{60:40}$ film exhibits no visible cracks and becomes highly smooth. These findings clearly illustrate that increasing the lignin-based epoxy resin content results in a shift from toughness to brittleness, which is consistent with the tensile mechanical results shown in Fig. 4e. Furthermore, as shown in Fig. 4f and g, the thermal stability of LEP-NIPUs films was analyzed using thermogravimetric analysis (TGA) and differential thermogravimetry (DTG), with the pertinent characteristic parameters listed in Table 4. The weight loss curves of all LEP-NIPUs films exhibit two distinct degradation phases. The initial phase ranging from 150 °C to 350 °C is attributed to the decomposition of lignin side chains and the cleavage of urethane bonds. The thermal degradation occurring between 350 °C and 550 °C is primarily related to the degradation of the cross-linked aromatic structure of LEP.[63] As shown in Table 4, LEP-NIPU samples retain higher residual carbon content at 600 °C compared to pristine NIPUs, with residual carbon content increasing proportionally with the LEP content. Conversely, the key thermal stability parameters such as the temperatures at 5% weight loss ($T_{5\%}$), 30% weight loss ($T_{30\%}$), the statistic heat-resistant index temperature (T_s), and the maximum decomposition temperature (T_{max}) exhibit a decreasing trend as the LEP content increases. As shown in Fig. 4h, LEP-NIPU films undergo a transition from a glassy state to a rubbery state with increasing temperature, reflecting the molecular chains' movement from a frozen to an unfrozen state. The temperature associated with the maximum peak in the tan δ curve is defined as the glass transition temperature (T_g). As depicted in Fig. 4i, T_g increases from 27 °C to 61 °C, which is attributed to the enhanced formation of network structures facilitated by the incorporation of LEP. The hydrophobicity of LEP-NIPU films towards seawater was evaluated through contact angle measurements using seawater. As illustrated in Fig. 4k, the LEP-NIPUs films exhibit seawater hydrophobicity. Notably, the contact angle exhibits a progressive augmentation in tandem with the successive increment of the LEP content. Corrosion resistance of the films under extreme seawater conditions was assessed by immersing four film samples in sealed glass bottles filled with seawater and boiling them at 63 °C for 3 h. The photographic images and corresponding residual rates before and after boiling (see Fig. S8a and b in the ESI†) demonstrate that all four LEP-NIPU films retained excellent structural integrity despite exposure to high-temperature seawater, with residual rates exceeding 99%.

Table 4 The TGA data of LEP-NIPU samples

Sample	$T_{5\%}$ (°C)	$T_{30\%}$ (°C)	T_s (°C)	T_{max} (°C)	C_{600} (%)
NIPUs	297.28	378.28	169.48	454.81	0.88
LEP-NIPU$_{60:40}$	279.31	392.31	170.08	449.43	10.50
LEP-NIPU$_{50:50}$	286.29	393.29	171.74	449.94	9.39
LEP-NIPU$_{40:60}$	286.24	394.24	172.01	450.44	7.59
LEP-NIPU$_{30:70}$	291.33	395.33	173.33	450.92	5.09

T_s was calculated using the equation: $T_s = 0.49\ [T_{5\%} + 0.6\ (T_{30\%} - T_{5\%})]$.

The non-isothermal curing behaviors of the LEP-NIPU systems were analyzed using DSC. Fig. 5 displays the DSC curves of the LEP-NIPUs at various heating rates (5, 10, 15, 20, and 25 °C min^{-1}), with the corresponding data summarized in Table S3 of the ESI.† Fig. 5a–d indicate that all LEP-NIPU films exhibit a distinct exothermic peak at different heating rates. This observation implies that the curing reaction between lignin-based epoxy resins and primary amines occurs in a single step and remains unaffected by the constituent proportions.[64] Moreover, the exothermic peak of the curing reaction shifts to higher temperatures, with the peak value increasing progressively as the heating rate rises. This behavior can be attributed to the fact that the exothermic reaction proceeds more gently at a lower heating rate and provides the system with adequate time to complete the reaction. As the heating rate progressively increases, the thermal effect generated by the system concomitantly intensifies, thereby resulting in a more pronounced temperature difference and causing the exothermic peak to shift to higher temperatures. Subsequently, this prompts the exothermic peak of the curing reaction to shift towards a higher temperature. As depicted in Fig. 5e, f and Table S4 of the ESI,† the apparent activation energy (E_a) values of the LEP-NIPUs were calculated using the Kissinger and Ozawa equations based on the peak temperatures (T_p).[65,66] The E_a value typically represents the energy barrier of a reaction, defined as the minimum energy required for a chemical reaction to occur.[67] The E_a of LEP-NIPU$_{30:70}$ is 68.16 kJ mol^{-1}, with a gradual decrease observed as the proportion of LEP increases and that of NIPUs decreases. These results indicate that the incorporation of LEP significantly promotes the curing reaction within the whole system.

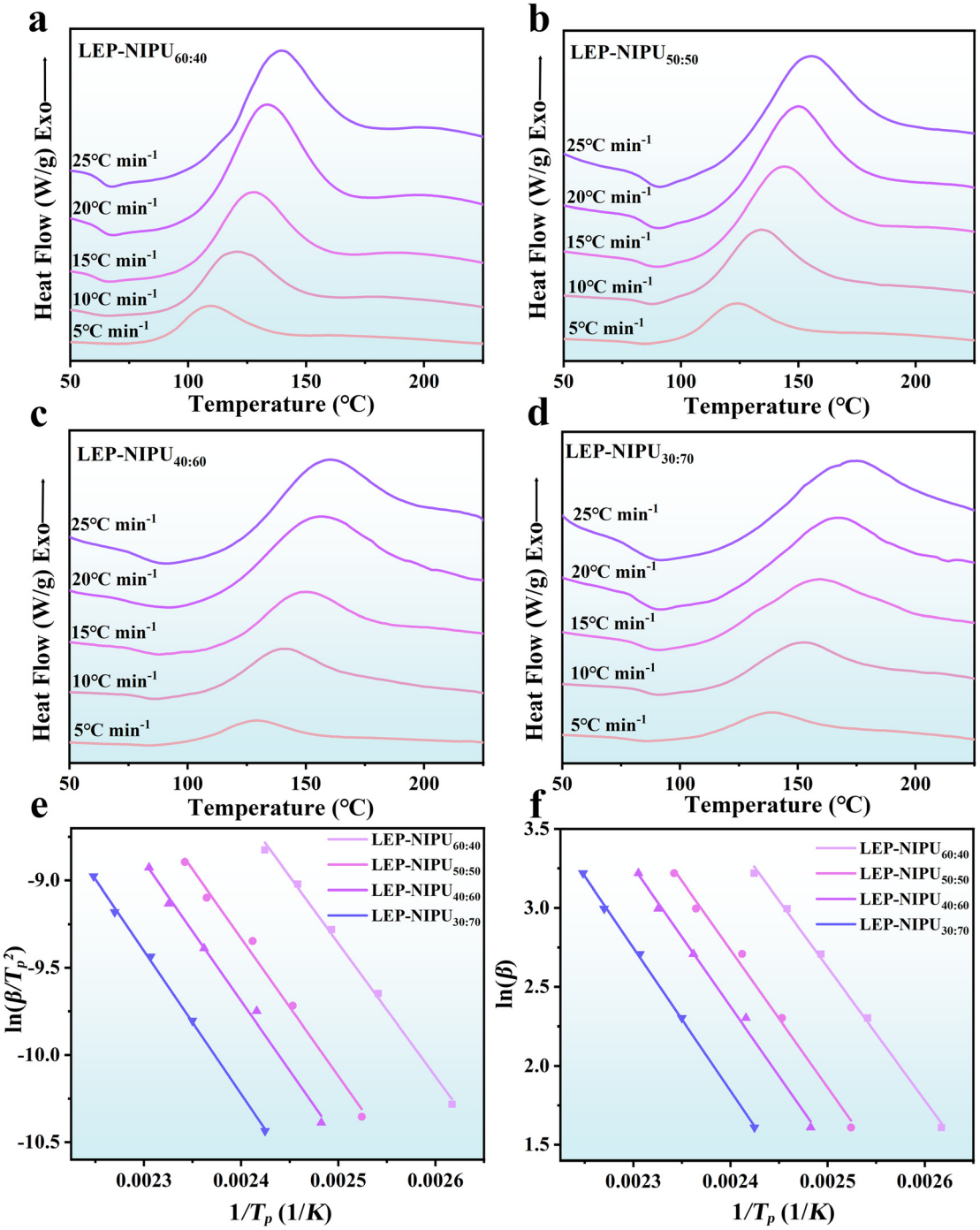

Fig. 5 DSC curves of LEP-NIPUs at heating rates of 5, 10, 15, 20 and 25 °C min^{-1}: (a) $LEP\text{-}NIPU_{60:40}$, (b) $LEP\text{-}NIPU_{50:50}$, (c) $LEP\text{-}NIPU_{40:60}$, and (d) $LEP\text{-}NIPU_{30:70}$; (e) Kissinger and (f) Ozawa plots of LEP-NIPUs systems.

The curing process significantly influences the properties of the samples. Based on the results obtained from the curing reaction kinetics, it is essential to ascertain the optimal curing process parameters for the entire reaction system and to guarantee the excellent performance of the samples. The reaction rate of the curing reaction kinetics is described by eqn (1).[68]

$$d\alpha/dt = f(T) \times f(\alpha) = A \times (1-\alpha)^n \times \exp(-E_\alpha/RT_p). \quad (1)$$

$$d(\ln \beta)/d(1/T_p) \approx -E_a/nR \quad (2)$$

where A, n, and α refer to the pre-exponential factor, the order of curing reaction, and the conversion rate, respectively. The order of the curing reaction (n) is determined according to the Crane equation (eqn 2) by plotting the $\ln\beta - 1/T_P$ fitting curve. The calculated values of n are approximately 0.9, which indicate that the curing reaction is a complex process.[69] The

kinetic models of the curing reaction are shown in Table S5 of the ESI.† As shown in Fig. 6, the intercept of the fitting line of T against β represents the curing temperature of the curing system. The curing time is calculated by assuming a conversion rate (α) of 99% and substituting the curing temperature into the kinetic model of the curing reaction for each sample. To ensure complete curing of the samples without affecting their properties, the curing process is finalized as a reaction at 140 °C for 6 h (see Table S6 in the ESI†).

Fig. 7a illustrates the application of LEP-NIPU adhesives on plywood. Since the raw materials of the adhesives are derived from biomass and no toxic substances are emitted during the preparation process, the resulting plywood is environmentally friendly and suitable for indoor applications. Additionally, CO_2 generated from the manufacturing of plywood and other industrial processes can be utilized in the synthesis of adhesives, thereby achieving a circular utilization of CO_2 within the production process. The shearing strength test and wet shear strength results for various LEP-NIPU adhesives are shown in Fig. 7b–d. An increase in the LEP content and a decrease in the NIPU content result in a gradual rise in the wet shear strength of the plywood. This improvement is attributed to the fact that the rigidity of the whole material and the water resistance gradually augmented in tandem with the escalating content of LEP, thereby leading to the enhancement in the wet shear strength of the plywood. The wet shear strength of LEP-NIPU$_{60:40}$ can reach up to 2.31 MPa, whereas LEP-NIPU$_{30:70}$ can attain 1.74 MPa.

To address cost and time considerations of the adhesives for industrial applications, the glue application level and hot pressing parameters are optimized during the plywood manufacturing process. Reducing the glue application level from 240 g m^{-2} to 140 g m^{-2} decreases the wet bonding strength of LEP-NIPU$_{60:40}$ from 2.66 MPa to 2 MPa (Fig. 7e), which still meets the national standard for grade II plywood (≥0.7 MPa). Fig. 7f shows that when the glue application is controlled at 140 g m^{-2} and the hot pressing time is reduced from 15 min to 3 min, the wet bond strength of LEP-NIPU$_{60:40}$ decreases marginally from 2 MPa to 1.95 MPa, indicating that the duration of hot pressing time has a minimal effect on the wet bond strength. Therefore, considering the cost and time in practical applications, it is more appropriate to control the

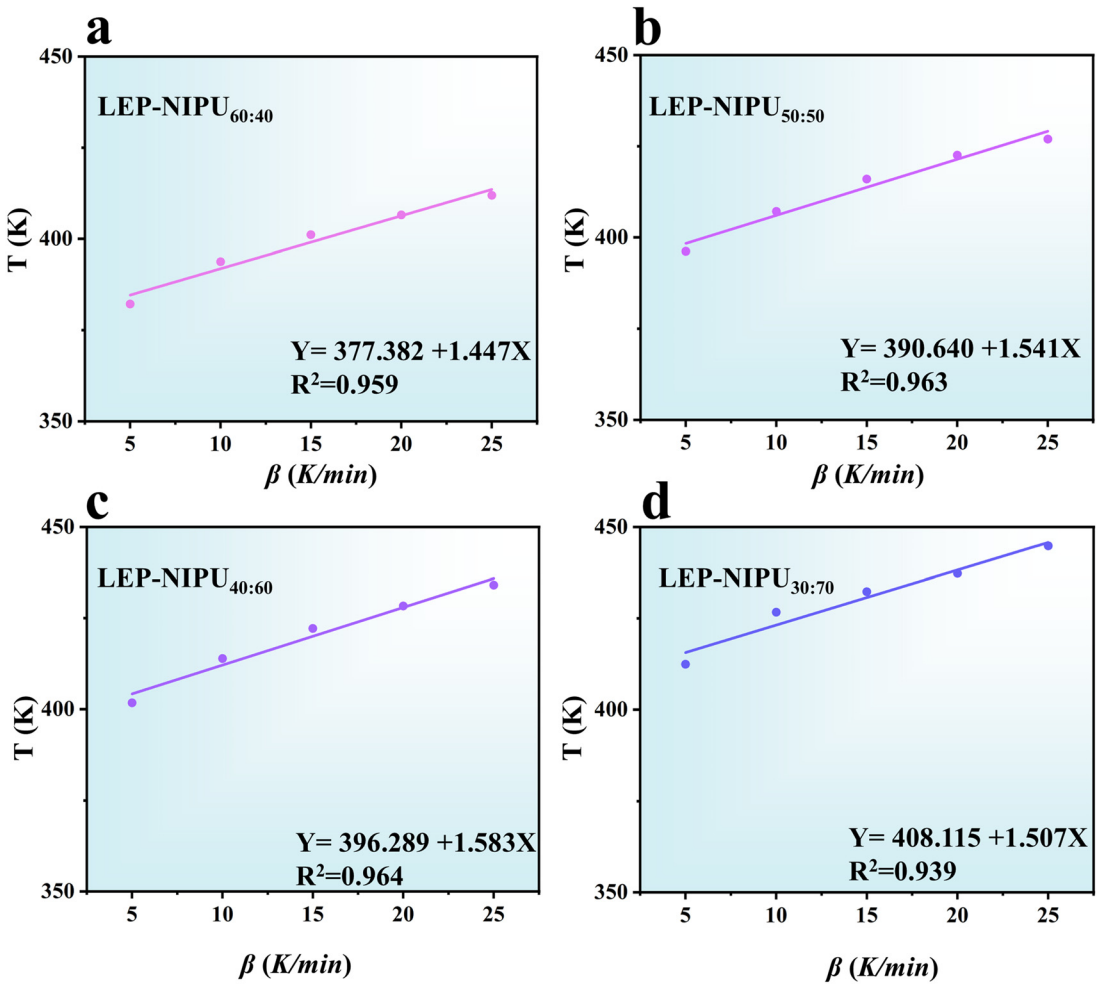

Fig. 6 T–β plots of the LEP-NIPUs systems: (a) LEP-NIPU$_{60:40}$, (b) LEP-NIPU$_{50:50}$, (c) LEP-NIPU$_{40:60}$, and (d) LEP-NIPU $_{30:70}$.

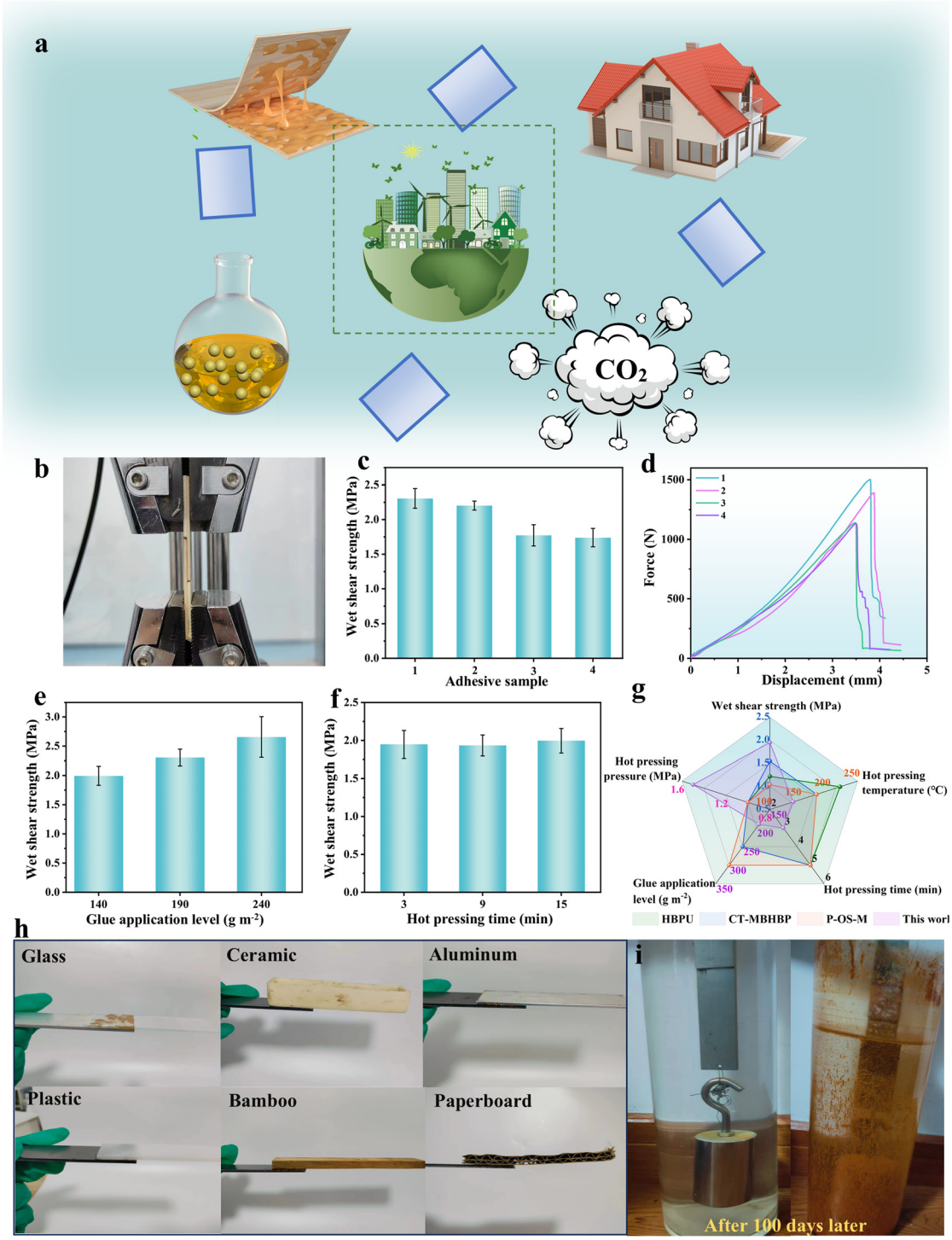

Fig. 7 (a) Schematic diagram of LEP-NIPU adhesives application in wood-based panels; (b) photograph of shearing strength test; (c) wet shear strength of various LEP-NIPU adhesives: 1 (LEP-NIPU$_{60:40}$), 2 (LEP-NIPU$_{50:50}$), 3 (LEP-NIPU$_{40:60}$), and 4 (LEP-NIPU$_{30:70}$); (d) force–displacement curves for wet shear strength; (e) effect of glue application level on wet shear strength; (f) effect of hot pressing time on wet shear strength; (g) comparison of the LEP-NIPU$_{60:40}$ adhesive with previously reported adhesives regarding glue application level, hot pressing pressure, hot pressing time, hot pressing temperature, and wet shear strength; (h) photographs of the LEP-NIPU$_{60:40}$ adhesive adhered to various substrates; (i) seawater adaptability of the LEP-NIPU$_{60:40}$ adhesive.

adhesives application level at 140 g m^{-2} and limit the hot pressing time to 3 min. Fig. 7g presents a comparative analysis of LEP-NIPU$_{60:40}$ adhesives with other adhesives across various parameters including hot pressing time, adhesives application level, hot pressing temperature, pressing pressure, and wet bond strength. These results indicate that LEP-NIPU$_{60:40}$

adhesives exhibit a significantly higher wet bond strength than other adhesives, even with a reduced adhesive application level, lower hot pressing temperature, and shorter hot pressing time. This highlights its substantial potential for advancing adhesives technology.

Additionally, the application of LEP-NIPU adhesives can be further expanded in other fields by testing the interfacial adhesion performance on various materials. The LEP-NIPU$_{60:40}$ adhesive adhered effectively to various substrates, including glass, ceramic, aluminum sheets, plastic, bamboo, and paperboard, indicating excellent interfacial bonding capabilities and significant prospects for application in the bonding of other substrates (Fig. 7h). Simultaneously, its corrosion resistance in seawater was evaluated by coating steel plates (100 mm × 25 mm × 2 mm) over an area of 25 mm × 25 mm. The adhesive application level was 140 g m^{-2}, followed by hot pressed at 140 °C for 3 min. After cooling at room temperature for 24 h, the plates were immersed in seawater with a 500 g calibration weight suspended at the bottom. Fig. 7i demonstrates that the adhesives still firmly bonded the steel plates even after 100 days, indicating excellent corrosion resistance in seawater. Fig. S9 of the ESI† shows the photographs of the LEP-NIPU$_{60:40}$ adhesive adhered with various substrate materials (rubber, ceramic, agate, glass, bamboo, and plastic) under seawater conditions, highlighting its versatility in such environments.

4. Conclusions

In summary, green, bio-based NIPU adhesives with superior bonding strength and excellent water resistance have been successfully synthesized. This was achieved through the formation of a robust three-dimensional reticulated structure resulting from the reaction of linear NIPUs, derived from biomass materials and CO_2, with lignin-based epoxy resin. In this structure, the epoxy resin functions as the rigid segments, while the NIPUs serve as the flexible segments. The resulting material demonstrates remarkable mechanical properties, including a tensile strength of up to 20.01 MPa, along with excellent hydrophobicity and resistance to seawater corrosion. By adjusting the ratio between NIPUs and LEP, polymers with varying mechanical strengths can be obtained, with optimal tensile strength observed when LEP constituted 60% of the total molar amount. Furthermore, the LEP-NIPU$_{60:40}$ adhesives, when applied as the wood adhesives, achieve a wet strength of 1.95 MPa with an adhesive application level of 140 g m^{-2} and a hot pressing time of 3 min. Therefore, the polymer not only advances the high-value utilization of green biomass materials and CO_2 greenhouse gases but also serves as a valuable reference for designing underwater adhesives, offering significant prospects for broader applications.

Author contributions

Ping Zhang: investigation, methodology, data curation, and writing – original draft. Chen Qin: supervision, formal analysis, and data curation. Hao Yuan: data analysis. Yu Wang: investigation and validation. Yizhong Cao: investigation and validation. Zhe Wang: conceptualization, methodology, writing – review & editing, and supervision. Chunde Jin: methodology, project administration, supervision, conceptualization, and funding acquisition.

Data availability

The data supporting this article have been included as part of the ESI.†

Conflicts of interest

The authors declare no competing financial interest.

Acknowledgements

This work was supported by the Natural Science Foundation of Zhejiang Province (LZ23C160004).

References

1 Z. Liu, X. Zhang, W. Zhou, G. Wang, T. Liu, J. Luo, Q. Gao, J. Luo and J. Li, *J. Cleaner Prod.*, 2023, **414**, 137739.
2 J. Liu, Y. Li, H. Mo, E. Xie, J. Fang and W. Gan, *J. Ind. Eng. Chem.*, 2022, **115**, 48–61.
3 J. Wang, R. Wang, X. Ji, C. Jin and Y. Yan, *J. Mater. Res. Technol.*, 2023, **26**, 8213–8228.
4 *Phenolic resins: A century of progress*, ed. L. Pilato, Springer, Berlin, Heidelberg, 2010.
5 D. Gonçalves, J. M. Bordado, A. C. Marques and R. Galhano dos Santos, *Polymers*, 2021, **13**, 4086.
6 R. J. Li, J. Gutierrez, Y.-L. Chung, C. W. Frank, S. L. Billington and E. S. Sattely, *Green Chem.*, 2018, **20**, 1459–1466.
7 J. Niesiobędzka and J. Datta, *Green Chem.*, 2023, **25**, 2482–2504.
8 L. Passauer, *Prog. Org. Coat.*, 2021, **157**, 106331.
9 Y. Wu, T. Wang, J. Gao, L. Zhang, J. D. B. Fay, S. Hirth, J. Hankett and Z. Chen, *Langmuir*, 2023, **39**, 3273–3285.
10 O. Kreye, H. Mutlu and M. A. R. Meier, *Green Chem.*, 2013, **15**, 1431.
11 S. S. Bhattacharyya, F. F. G. D. Leite, M. A. Adeyemi, A. J. Sarker, G. S. Cambareri, C. Faverin, M. P. Tieri, C. Castillo-Zacarias, E. M. Melchor-Martinez, H. M. N. Iqbal and R. Parra-Saldivar, *Sci. Total Environ.*, 2021, **790**, 148169.
12 R. Newman and I. Noy, *Nat. Commun.*, 2023, **14**, 6103.
13 M. M. F. Hasan, L. M. Rossi, D. P. Debecker, K. C. Leonard, Z. Li, B. C. E. Makhubela, C. Zhao and A. Kleij, *ACS Sustainable Chem. Eng.*, 2021, **9**, 12427–12430.

14 S. Motokucho, Y. Takenouchi, R. Satoh, H. Morikawa and H. Nakatani, *ACS Sustainable Chem. Eng.*, 2020, **8**, 4337–4340.
15 A. Rehman, F. Saleem, F. Javed, A. Ikhlaq, S. W. Ahmad and A. Harvey, *J. Environ. Chem. Eng.*, 2021, **9**, 105113.
16 X. Ou, Y. Niu, Q. Liu, L. Li, F. Wei, Y. Cui, Y. Zhou and F. Yan, *Prog. Polym. Sci.*, 2024, **149**, 101780.
17 O. Kreye, H. Mutlu and M. A. R. Meier, *Green Chem.*, 2013, **15**, 1431.
18 K. Błażek and J. Datta, *Crit. Rev. Environ. Sci. Technol.*, 2019, **49**, 173–211.
19 X. Yang, C. Ren, X. Liu, P. Sun, X. Xu, H. Liu, M. Shen, S. Shang and Z. Song, *Mater. Chem. Front.*, 2021, **5**, 6160–6170.
20 Y. Zhou, F. Dong, X. Chen, X. Huang, L. Guo, H. Liu and X. Xu, *Ind. Crops Prod.*, 2024, **211**, 118203.
21 Y. Yang, H. Cao, Y. Wang, J. Zhao, W. Ren, B. Wang, P. Qin, F. Chen, Y. Wang and D. Cai, *Ind. Crops Prod.*, 2022, **186**, 115224.
22 M. Bähr, A. Bitto and R. Mülhaupt, *Green Chem.*, 2012, **14**, 1447–1454.
23 P. Sruthi and M. M. Naidu, *Food Chem.*, 2023, **3**, 100390.
24 H. A. Klfout, A. M. Asiri, K. A. Alamry and M. A. Hussein, *RSC Adv.*, 2023, **13**, 19817–19835.
25 K. Makwana, A. B. Ichake, V. Valodkar, G. Padmanaban, M. V. Badiger and P. P. Wadgaonkar, *Eur. Polym. J.*, 2022, **166**, 111029.
26 C. Bo, Y. Sha, F. Song, M. Zhang, L. Hu, P. Jia and Y. Zhou, *J. Cleaner Prod.*, 2022, **341**, 130898.
27 X. Liu, X. Yang, S. Wang, S. Wang, Z. Wang, S. Liu, X. Xu, H. Liu and Z. Song, *ACS Sustainable Chem. Eng.*, 2021, **9**, 4175–4184.
28 B. Zhang, X. Yang, X. Lin, H. Shang, Q. Liu, H. Wang, S. Liu, X. Xu and F. Dong, *ACS Sustainable Chem. Eng.*, 2023, **11**, 6100–6113.
29 Y. Zhou, F. Dong, X. Chen, X. Huang, L. Guo, H. Liu and X. Xu, *Ind. Crops Prod.*, 2024, **211**, 118203.
30 B. Bizet, E. Grau, J. M. Asua and H. Cramail, *Macromol. Chem. Phys.*, 2022, **223**, 2100437.
31 J. Ke, X. Li, F. Wang, S. Jiang, M. Kang, J. Wang, Q. Li and Z. Wang, *RSC Adv.*, 2017, **7**, 28841–28852.
32 X. He, X. Xu, Q. Wan, G. Bo and Y. Yan, *Polymers*, 2017, **9**, 649.
33 X. Yu, B. Yang, W. Zhu, T. Deng, Y. Pu, A. Ragauskas and H. Wang, *Ind. Crops Prod.*, 2023, **200**, 116824.
34 S. Gillet, M. Aguedo, L. Petitjean, A. R. C. Morais, A. M. da Costa Lopes, R. M. Lukasik and P. T. Anastas, *Green Chem.*, 2017, **19**, 4200–4233.
35 A. E. Kazzaz, Z. H. Feizi and P. Fatehi, *Green Chem.*, 2019, **21**, 5714–5752.
36 H. Zhou, J. Y. Xu, Y. Fu, H. Zhang, Z. Yuan, M. Qin and Z. Wang, *Green Chem.*, 2019, **21**, 4625–4632.
37 T. Li, B. Zhang, S. Jiang, X. Zhou, G. Du, Z. Wu, M. Cao and L. Yang, *ACS Sustainable Chem. Eng.*, 2020, **8**, 5209–5216.
38 S. L. Sunar, R. K. Oruganti, D. Bhattacharyya, D. Shee and T. K. Panda, *Cellulose*, 2024, **31**, 2151–2173.
39 J. Ouyang, W.-Q. He, Q.-M. Li, L. Chen, X.-F. Wu and X.-J. Su, *Appl. Sci.*, 2022, **12**, 1432.
40 W. Yang, E. Fortunati, D. Gao, G. M. Balestra, G. Giovanale, X. He, L. Torre, J. M. Kenny and D. Puglia, *ACS Sustainable Chem. Eng.*, 2018, **6**, 3502–3514.
41 I. Dudeja, R. K. Mankoo, A. Singh and J. Kaur, *Int. J. Food Sci. Technol.*, 2023, **58**, 2754–2763.
42 W. Guo, S. Sun, P. Wang, H. Chen, J. Zheng, X. Lin, Y. Qin and X. Qiu, *Int. J. Biol. Macromol.*, 2022, **221**, 913–922.
43 R. Tang, B. Xue, J. Tan, Y. Guan, J. Wen, X. Li and W. Zhao, *ACS Appl. Polym. Mater.*, 2022, **4**, 1117–1125.
44 T. Pang, G. Wang, H. Sun, W. Sui and C. Si, *Ind. Crops Prod.*, 2021, **165**, 113442.
45 X.-Y. Li, L.-P. Xiao, S.-L. Zou, Q. Xu, Q. Wang, Y.-H. Lv and R.-C. Sun, *ACS Appl. Polym. Mater.*, 2023, **5**, 3611–3621.
46 C. Asada, S. Basnet, M. Otsuka, C. Sasaki and Y. Nakamura, *Int. J. Biol. Macromol.*, 2015, **74**, 413–419.
47 E. Feghali, D. J. van de Pas, A. J. Parrott and K. M. Torr, *ACS Macro Lett.*, 2020, **9**, 1155–1160.
48 X. Wang, W. Leng, R. M. O. Nayanathara, E. B. Caldona, L. Liu, L. Chen, R. C. Advincula, Z. Zhang and X. Zhang, *Int. J. Biol. Macromol.*, 2022, **221**, 268–277.
49 D. Ouyang, H. Chen, N. Liu, J. Zhang and X. Zhao, *Renewable Energy*, 2022, **185**, 196–207.
50 C. Gioia, G. Lo Re, M. Lawoko and L. Berglund, *J. Am. Chem. Soc.*, 2018, **140**, 4054–4061.
51 K. Wang, F. Xu and R. Sun, *Int. J. Mol. Sci.*, 2010, **11**, 2988–3001.
52 M. Balat, *Energy Sources, Part A*, 2008, **30**, 620–635.
53 M. J. Oren, M. M. Nassar and G. D. M. Mackay, *Can. J. Spectrosc.*, 1984, **29**, 10–12.
54 X. Jiang, D. Savithri, X. Du, S. Pawar, H. Jameel, H.-M. Chang and X. Zhou, *ACS Sustainable Chem. Eng.*, 2017, **5**, 835–842.
55 R. Tang, B. Xue, J. Tan, Y. Guan, J. Wen, X. Li and W. Zhao, *ACS Appl. Polym. Mater.*, 2022, **4**, 1117–1125.
56 H. Cao, R. Liu, B. Li, Y. Wu, K. Wang, Y. Yang, A. Li, Y. Zhuang, D. Cai and P. Qin, *Ind. Crops Prod.*, 2022, **177**, 114480.
57 Q. Cao, Q. Wu, L. Dai, X. Shen and C. Si, *Green Chem.*, 2021, **23**, 2329–2335.
58 Z. Ling and Q. Zhou, *Green Chem.*, 2023, **25**, 10082–10090.
59 Y. Zhang, L. Chu, Z. Dai, N. Bao, M. B. de Rooij, L. Gao, W. Tan and L. Shen, *Prog. Org. Coat.*, 2022, **171**, 107060.
60 T. Wang, H. Deng, N. Li, F. Xie, H. Shi, M. Wu and C. Zhang, *Green Chem.*, 2022, **24**, 8355–8366.
61 P. Miao, J. Liu, M. He, X. Leng and Y. Li, *Chem. Eng. J.*, 2023, **475**, 146398.
62 T. Wang, H. Deng, H. Zeng, J. Shen, F. Xie and C. Zhang, *ACS Sustainable Resour. Manage.*, 2024, **1**, 462–470.
63 T. Zhang, B. Xue, Q. Yan, Y. Yuan, J. Tan, Y. Guan, J. Wen, X. Li and W. Zhao, *Ind. Crops Prod.*, 2023, **199**, 116706.
64 J. Li, Z. Zhang, Y. Zhang, F. Sun, D. Wang, H. Wang and Z. Jin, *Int. J. Biol. Macromol.*, 2021, **192**, 516–524.
65 G. Lou, Q. Rao, Q. Li, Z. Bai, X. He, Y. Xiao, J. Dai, S. Fu and S. Yang, *Chem. Eng. J.*, 2023, **455**, 139334.

66 Y. Zhang, J. Li, X. Wu, D. Wang, S. Zhou, S. Han, H. Wang and F. Sun, *Int. J. Biol. Macromol.*, 2022, **217**, 243–254.
67 M. Rojas, D. Ruano, E. Orrego-Restrepo and F. Chejne, *Biomass Bioenergy*, 2023, **177**, 106932.
68 M. R. Firouzmanesh and A. A. Azar, *J. Reinf. Plast. Compos.*, 2005, **24**, 345–353.
69 Q. Liang, X.-P. Feng, K. Zhang, X.-M. Hui, X. Hou and J.-R. Ye, *Polymer*, 2022, **256**, 125162.